Four Dimensional Real Time Kinematic State Estimation and Analysis of Relative Clock Solutions

Yanming Feng
Queensland University of Technology, Australia
Bofeng Li
Tongji University, P.R. China

BIOGRAPHY

Yanming Feng is a Professor of Queensland University of Technology in Brisbane Australia where he is responsible for a research group for wireless communications and GNSS navigation. In recent years, he has been a project leader for a number of Australian Cooperative Research Centre (CRC) funded research programs including "Multi-GNSS data processing strategies and services" and "Wireless Communication Standard Framework". His active research interests include satellite orbit determination, real time kinematic positioning and timing, data processing of multiple GNSS frequency signals and Dedicated Short-Range Communications (DSRC) for road safety. He is the Editor-in-Chief for Journal of Global Positioning Systems. He received PhD degree in Satellite Geodesy from Wuhan Technical University of Surveying and Mapping (now part of Wuhan University), China in 1990.

Bofeng Li received his BSc. and PhD degree in Geodesy and Surveying Engineering from Tongji University, China, in 2005 and 2010 respectively. He is now a Research Fellow in GNSS research centre, Curtin University of Technology, Australia. His research interests include integer estimation and GNSS ambiguity resolution, Network RTK, Data processing theory of multiple frequency GNSS signals, Geodetic data processing theory etc. Dr. Li has published more than 40 peer-reviewed papers in GNSS and Geodetic data processing theory, and received more than 20 awards from different organizations including the ION GNSS 2008 sponsored student paper.

ABSTRACT

GNSS community has developed a series of GPS-based techniques for clock measurements and comparisons including time dissemination with the standard GPS point positioning method, clock synchronization using the code-based differential GPS positioning technique and using precise point positioning (PPP) for clock comparison. In the mean time, significant advances have been made towards real time kinematic (RTK) positioning which enables three dimensional (3D) positioning at centimeter accuracy, but without clock solutions. This paper presents a four dimensional real time kinematic (4D-RTK) method, which provides RTK timing solutions for applications such as clock synchronization and remote clocks steering in addition to 3D RTK position solutions as usual. The proposed 4D RTK model is based on *n* single differenced (SD) measurements between receivers for a baseline with (*n*-1) double differenced (DD) integer constraints. The existing 3D RTK model use (*n*-1) DD code and phase measurements can only enable position estimation, eliminating the receiver clock errors. In the 4D RTK, the user 3D position states are determined as usual with the DD phase measurements whose integer ambiguities are searched and fixed using the existing integer least squares (ILS) procedure. Estimation of the relative clock bias and SD phase biases is based on the SD code and phase observational equations. The constant nature of the SD phase ambiguity biases is used to improve the SD phase bias from epoch to epoch, and thus the relative clock solutions. The 4D RTK can be simplified to a RTK timing problem if the user baselines are given. Experimental analysis has been performed with a GPS data set collected over a 21 km baseline at 15 second interval for a total of 85 minutes. The results show that within the first few minutes of observations, the SD phase biases fall within the range of 0.3 cycles, thus resulting in the clock uncertainty of 0.1 to 0.2 ns. Beyond 150 epochs (about 40 minutes), the SD phase biases are stabilized within the range of 0.1 cycle, thus the clock biases can be estimated to the precision and accuracy of better than 0.1 ns, including the effect of the errors in the SD phase measurements. In general RTK timing has a significant potential for high precision real time clock synchronizations over very long distances.

1. INTRODUCTION

With sufficient number of Global Navigation Satellite System (GNSS) code and phase measurements, user state parameters, position, velocity and time (PVT), can be estimated at the different accuracy levels. Significant advances have been made towards the improvement of real time position estimation to accuracy down to the centimeter level using techniques such as precise point positioning (PPP) and real time kinematic (RTK)

23rd International Technical Meeting of the Satellite Division of
The Institute of Navigation, Portland, OR, September 21-24, 2010

positioning in the past two decades. GNSS community has developed a series of GPS-based techniques for clock measurements and comparisons since early 1980s, including the contributions by Allan et al (1980), Lewandowski et al (1991) and Miranian et al (1991). The simplest GNSS time transfer method is GPS being used as a clock in the one-way mode (OWM) where a single GPS receiver is anywhere to provide clock solutions at the precision and accuracy of 20-30 ns since selective availability turned to zero in 2000. Parker et al (2004) outlined the advances in time and frequency dissemination using GPS techniques. The second method is to use the differential GPS to synchronize two clocks separated by large distances in the common-view mode to the precision and accuracy of 5-10 ns. Schildknecht (2000) examined the high precision time and frequency transfer using GPS phase measurements. Another way to synchronize clocks is the melting-pot method (MPM), which is similar to both OWM and CVM methods, but allows clocks at remote sites to be automatically controlled and steered. The latest technique is PPP, a technique initially developed for determining positions with sub-decimeter accuracy from single-receiver measurements. PPP offers high-level performance comparable with state-of-the-art methods, such as Two-Way Satellite Time and Frequency Transfer (TWSTFT), autonomously allowing recovery of the IGS combined clock solution at sub-nanosecond level (Orgiazzi et al). In general, if PPP technique can provide positioning solutions of centimeters in real time, it is possible provide real time clock solutions to the RMS accuracy of 0.1 ~0.3 ns with an advanced data processing system and the RMS is of 0.130 ns as shown in (ibid). Using precise GPS orbit and clocks for precise user clock estimations has attracted a significant research attention within the International GNSS Services (IGS) community, referring to the contributions by Kouba et al (2001) and Ray et al (2002, 2003). The advantages of PPP time solutions is that the user can directly obtain the time solutions in the UTC frame, considering the leap seconds between GPS time and UTC time. The disadvantages of PPP include long convergence time for desirable accuracy and higher latency of solutions with respect to RTK solutions. However, currently, RTK solutions are limited to 3D coordinates.

This paper presents a four-dimensional real time kinematic (4D-RTK) positioning and timing method, which provides precise relative clock solutions for applications such as synchronization and automation of remote clocks steering. The paper presents models and algorithms for 4D-RTK timing and experimental results. 4D RTK is a relative 3D positioning plus 1D timing concept. In Section 2, the rigorous 4D RTK models and algorithms are given, which are based on *n* between-receiver single differenced (SD) measurements for a baseline with (*n*-1) double differenced (DD) integer constraints. Section 3 examines the effects of inter-frequency and inter-receiver biases on the relative clock solutions. Section 4 gives experimental analysis with a data set of 21 km baseline, showing that within a few minutes of observations, the relative clock bias can coverage to the accuracy of a few centimeters, that is, 0.1~0.2 ns. The final section concludes the paper with a summary of findings in this contribution.

2. 4D RTK models and algorithms

The 4D RTK is based on the between-receiver SD phase and code measurements. For simplicity, the linear equations for SD phase measurements are expressed as

$$\begin{bmatrix} L_{1,k} \\ \vdots \\ L_{n,k} \end{bmatrix} = \begin{bmatrix} a_{1,k} \\ \vdots \\ a_{n,k} \end{bmatrix} \delta X_k + c\delta T_k + \lambda \begin{bmatrix} N_1 \\ \vdots \\ N_n \end{bmatrix} + \begin{bmatrix} \varepsilon_{L_{1,k}} \\ \vdots \\ \varepsilon_{L_{n,k}} \end{bmatrix} \quad (1)$$

where there are *n* satellites in view at the *k*th epoch; L_i is the *i*th SD phase measurement for an original phase signal L1, or a combined signal from L1 and L2, which is contaminated by random error ε_{L_i} and inter-frequency-bias, and a_i is a 1×3 cosine vector for direction from satellite to receiver; δX, δT and N_i are 3D coordinate unknowns, SD clock error and the *i*th SD ambiguity with initial phase bias which are presented in real values; *c* is the light speed and λ is the wavelength of the carrier phase signal L_i at its frequency. The subscript *k* denotes the kth epoch. Similarly, the linear equations for code measurements is given

$$\begin{bmatrix} P_{1,k} \\ \vdots \\ P_{n,k} \end{bmatrix} = \begin{bmatrix} a_{1,k} \\ \vdots \\ a_{n,k} \end{bmatrix} \delta X_k + c\delta T_k + \begin{bmatrix} \varepsilon_{P_{1,k}} \\ \vdots \\ \varepsilon_{P_{n,k}} \end{bmatrix} \quad (2)$$

where $P_{i,k}$ is the ith SD code measurement for the P1 (or C/A) code, or combined measurement from P1 and P2 as shown in Table 1; ε_{P_i} is its random error. The remaining variables have the same meanings as those in equation (1). The equations (1) and (2) for phase and code measurements are obtained from standard SD processing between receivers, where (2) is the typical code based differential GPS model. In 4D RTK processing, the position and receiver clock parameters vary from epoch to epoch without dependences on clock models, but the SD ambiguity remains stable and generally treated as constant over a certain time interval. The SD observation equations at the *k*th epoch in matrix form reads

$$\mathbf{y}_k = \begin{bmatrix} \tilde{\mathbf{A}}_k & \tilde{\mathbf{B}} \end{bmatrix} \begin{bmatrix} \boldsymbol{\delta z}_k \\ \mathbf{N} \end{bmatrix} + \boldsymbol{\varepsilon}_{\mathbf{y}_k}, \quad \sigma_0^2 \mathbf{Q} = \sigma_0^2 \begin{bmatrix} \mathbf{Q}_L & \mathbf{0} \\ \mathbf{0} & \mathbf{Q}_P \end{bmatrix} \quad (3)$$

where

23rd International Technical Meeting of the Satellite Division of
The Institute of Navigation, Portland, OR, September 21-24, 2010

$$\mathbf{y}_k = \begin{bmatrix} L_{1,k} & \cdots & L_{n,k} & P_{1,k} & \cdots & P_{n,k} \end{bmatrix}^T ,$$

$$\boldsymbol{\delta z}_k = \begin{bmatrix} \delta X_k \\ \delta T_k \end{bmatrix}, \mathbf{N} = \begin{bmatrix} N_1 \\ \vdots \\ N_n \end{bmatrix}, \ \mathbf{A}_k = \begin{bmatrix} a_{1,k} \\ \vdots \\ a_{n,k} \end{bmatrix}$$

$$\tilde{\mathbf{A}}_k = \begin{bmatrix} 1 \\ 1 \end{bmatrix} \otimes \begin{bmatrix} \mathbf{A}_k & \mathbf{e} \end{bmatrix}, \ \tilde{\mathbf{B}} = \begin{bmatrix} \lambda \mathbf{I}_n \\ \mathbf{0} \end{bmatrix}, \mathbf{B} = \lambda \mathbf{I}_n$$

where $\boldsymbol{I}_n$ is identity matrix with n dimension; σ_0^2 is the variance of unit weight for SD phase observation and $\boldsymbol{Q}_L$ is its cofactor matrix as of the covariance matrix $\sigma_0^2 \mathrm{Q}_\mathrm{L}$. The cofactor matrix $\boldsymbol{Q}_P$ of SD pseudoranges is satisfied with $\mathbf{Q}_P = \sigma_P^2 / \sigma_0^2 \times \mathbf{Q}_L$,where σ_P^2 is the variance of the SD pseudorange noise. It is important to notice that we use δT_k in meter to denote $c\delta T_k$. The LS solution of the SD observation equation system (3) is

$$\begin{bmatrix} \boldsymbol{\delta}\hat{\mathbf{z}}_k \\ \hat{\mathbf{N}} \end{bmatrix} = \begin{bmatrix} \tilde{\mathbf{A}}_k^T \mathbf{Q}^{-1} \tilde{\mathbf{A}}_k & \tilde{\mathbf{A}}_k^T \mathbf{Q}^{-1} \tilde{\mathbf{B}} \\ \tilde{\mathbf{B}}^T \mathbf{Q}^{-1} \tilde{\mathbf{A}}_k & \tilde{\mathbf{B}}^T \mathbf{Q}^{-1} \tilde{\mathbf{B}} \end{bmatrix}^{-1} \begin{bmatrix} \tilde{\mathbf{A}}_k^T \mathbf{Q}^{-1} \mathbf{y}_k \\ \tilde{\mathbf{B}}^T \mathbf{Q}^{-1} \mathbf{y}_k \end{bmatrix} \quad (4)$$

In general, measurements from multiple epochs would be cumulated for the SD ambiguity solutions. For simplicity, $\boldsymbol{\delta z}_k$ is equivalently eliminated for each epoch and only SD ambiguity parameters are retained, i.e.,

$$\mathbf{R}_k \mathbf{y}_k = \mathbf{R}_k \tilde{\mathbf{B}} \mathbf{N} + \boldsymbol{\varepsilon}_{\mathbf{y}_k} \quad (5)$$

where the transformation matrix

$$\mathbf{R}_k = \mathbf{I} - \tilde{\mathbf{A}}_k \left(\tilde{\mathbf{A}}_k^T \mathbf{Q}^{-1} \tilde{\mathbf{A}}_k \right)^{-1} \tilde{\mathbf{A}}_k^T \mathbf{Q}^{-1}$$

which is an idempotent matrix satisfying with $\mathbf{R}_k \mathbf{R}_k = \mathbf{R}_k$, $\mathbf{Q}^{-1} \mathbf{R}_k = \mathbf{R}_k^T \mathbf{Q}^{-1}$ and $\mathbf{Q}^{-1} \mathbf{R}_k = \mathbf{R}_k^T \mathbf{Q}^{-1}$.

With measurements cumulated over the most current m epochs, the normal equations associated to the observation equation (5) are

$$\mathbf{Q}_{\hat{\mathbf{N}}}^{-1} \hat{\mathbf{N}} = \mathbf{w} \quad (6a)$$

where the cofactor matrix of SD ambiguities is

$$\mathbf{Q}_{\hat{\mathbf{N}}} = \left(\tilde{\mathbf{B}}^T \mathbf{Q}^{-1} \sum_{k=1}^{m} \mathbf{R}_k \tilde{\mathbf{B}} \right)^{-1} \quad (6b)$$

and the constant term

$$\mathbf{w} = \tilde{\mathbf{B}}^T \mathbf{Q}^{-1} \sum_{k=1}^{m} \mathbf{R}_k \mathbf{y}_k \quad (6c)$$

Thus the LS solution is

$$\hat{\mathbf{N}} = \mathbf{Q}_{\hat{\mathbf{N}}} \times \mathbf{w} \quad (6d)$$

To deal with the situation where a satellite is added or removed, we arrange the observations into two groups. At the current epoch m, the matrices $\boldsymbol{Q}$, $\tilde{\boldsymbol{B}}$ and $\boldsymbol{y}_k$, are expressed as follows

$$\boldsymbol{Q} = \begin{bmatrix} \boldsymbol{Q}_1 & 0 \\ 0 & \boldsymbol{Q}_2 \end{bmatrix}, \tilde{\boldsymbol{B}} = \begin{bmatrix} \tilde{\boldsymbol{B}}_1 \\ \tilde{\boldsymbol{B}}_2 \end{bmatrix}, \boldsymbol{y}_m = \begin{bmatrix} \boldsymbol{y}_1 \\ \boldsymbol{y}_2 \end{bmatrix}_m$$

The subscript '1' represents the group 1 satellites which are common to two consecutive epochs, and the subscript "2" the group 2 satellites which are either added or removed at the current epoch. In the case when the group 2 satellites are added, the sum of the matrices in (6b) is expressed as

$$\begin{bmatrix} \sum_{k=1}^{m-1} \boldsymbol{R}_k & 0 \\ 0 & 0 \end{bmatrix} + \begin{bmatrix} \boldsymbol{R}_{11} & \boldsymbol{R}_{12} \\ \boldsymbol{R}_{12} & \boldsymbol{R}_{22} \end{bmatrix}_m$$

and the sum of the vectors becomes in (6c) is

$$\begin{bmatrix} \sum_{k=1}^{m-1} \boldsymbol{R}_k \boldsymbol{y}_k & 0 \\ 0 & 0 \end{bmatrix} + \begin{bmatrix} \boldsymbol{R}_{11} & \boldsymbol{R}_{12} \\ \boldsymbol{R}_{12} & \boldsymbol{R}_{22} \end{bmatrix}_m \begin{bmatrix} \boldsymbol{y}_1 \\ \boldsymbol{y}_2 \end{bmatrix}_m$$

In the case when the group 2 satellites are removed, the sum of the matrices in (6b) will become

$$\left(\sum_{k=1}^{m-1} \boldsymbol{R}_k \right)_1 + \left[\boldsymbol{R}_{11} \right]_m$$

where the first term represents the sub-matrix including the columns and rows related to the group 1 satellites only. Similarly, the sum of the vectors in (6c) is given as

$$\left(\sum_{k=1}^{m-1} \boldsymbol{R}_k \boldsymbol{y}_k \right)_1 + \left[\boldsymbol{R}_{11} \boldsymbol{y}_1 \right]_m$$

where the first term represents the sub-vector including components only related to the group 1 satellites.

It is important to note that SD ambiguities N are real-valued due to the effects of initial phase biases and other receiver-specific biases, such as initial phase errors, but their differences amongst the satellites are integers in theory. To achieve more precise SD ambiguity and thus user state solutions, these integer constraints should be applied. Assuming the first satellite to be the reference satellite, we derive the DD float ambiguity solution by multiplying the DD operation matrix $\mathbf{D} = \begin{bmatrix} -\mathbf{e}_{n-1} & \mathbf{I}_{n-1} \end{bmatrix}$ to SD ambiguity solution, namely, the LS DD float solution is

$$\Delta\hat{\mathbf{N}} = \mathbf{D} \times \hat{\mathbf{N}} \quad (7a)$$

and its cofactor matrix is

$$\mathbf{Q}_{\Delta\hat{\mathbf{N}}} = \mathbf{D} \mathbf{Q}_{\hat{\mathbf{N}}} \mathbf{D}^T \quad (7b)$$

The DD ambiguities $\Delta\mathbf{N}$ is then determined by solving the following minimization problem

$$\Delta\breve{\mathbf{N}} = \arg \min_{\Delta\mathbf{N} \in \mathbb{Z}^{n-1}} \left(\Delta\mathbf{N} - \Delta\hat{\mathbf{N}} \right)^T \mathbf{Q}_{\Delta\hat{\mathbf{N}}}^{-1} \left(\Delta\mathbf{N} - \Delta\hat{\mathbf{N}} \right) \quad (8)$$

The search space is governed by the covariance matrix $\sigma_0^2 \mathbf{Q}_{\Delta\hat{\mathbf{N}}}$ and the strong correlation within $\mathbf{Q}_{\Delta\hat{\mathbf{N}}}$ can lead to larger search space. With the well-established decorrelation technique such as LAMBDA, the integer search can be completed quickly.

Once the fixed integer solutions $\Delta\breve{\mathbf{N}}$ are obtained, we can follow two approaches to derive the 3D and position and relative clock solutions. The first approach is to impose

the constraints $\mathbf{D}\times\mathbf{N}=\Delta\breve{\mathbf{N}}$ upon observation equations (5), the normal equations (6a) are updated to include these constraints as

$$\begin{bmatrix}\mathbf{Q}_{\hat{\mathbf{N}}}^{-1} & -\mathbf{D}^T\\ \mathbf{D} & \mathbf{0}\end{bmatrix}\begin{bmatrix}\hat{\mathbf{N}}_C\\ \hat{\mathbf{k}}\end{bmatrix}=\begin{bmatrix}\mathbf{w}\\ \Delta\breve{\mathbf{N}}\end{bmatrix} \tag{9}$$

Thus the solution of SD ambiguities with DD integer constraints becomes

$$\hat{\mathbf{N}}_C=\left(\mathbf{I}_n-\mathbf{Q}_{\hat{\mathbf{N}}}\mathbf{D}^T\mathbf{Q}_{\Delta\hat{\mathbf{N}}}^{-1}\mathbf{D}\right)\hat{\mathbf{N}}+\mathbf{Q}_{\hat{\mathbf{N}}}\mathbf{D}^T\mathbf{Q}_{\Delta\hat{\mathbf{N}}}^{-1}\Delta\breve{\mathbf{N}} \tag{10a}$$

and its cofactor matrix

$$\mathbf{Q}_{\hat{\mathbf{N}}_C}=\left(\mathbf{I}-\mathbf{Q}_{\hat{\mathbf{N}}}\mathbf{D}^T\mathbf{Q}_{\Delta\hat{\mathbf{N}}}^{-1}\mathbf{D}\right)\mathbf{Q}_{\hat{\mathbf{N}}}\left(\mathbf{I}-\mathbf{D}^T\mathbf{Q}_{\Delta\hat{\mathbf{N}}}^{-1}\mathbf{D}\mathbf{Q}_{\hat{\mathbf{N}}}\right) \tag{10b}$$

Some comments follow from (10a) and (10b) for SD ambiguity estimation. In principle the accuracy of SD ambiguity solution can be improved with the constraints of fixed DD integer ambiguities. However, to which degree the SD ambiguity can be improved with respect to its unconstrained estimate depends on the noise level of the SD ambiguity estimates. Substituting the SD ambiguity solution with constraints of DD integer ambiguities into the normal equations of the latest one epoch similar to (4), we compute the 4D parameters at the *m*th epoch

$$\delta\hat{\mathbf{z}}_m=\left(\tilde{\mathbf{A}}_m^T\mathbf{Q}^{-1}\tilde{\mathbf{A}}_m\right)^{-1}\left(\tilde{\mathbf{A}}_m^T\mathbf{Q}^{-1}\mathbf{y}_m-\tilde{\mathbf{A}}_m^T\mathbf{Q}^{-1}\tilde{\mathbf{B}}\hat{\mathbf{N}}_C\right) \tag{11a}$$

and their cofactor matrix

$$\mathbf{Q}_{\delta\hat{\mathbf{z}}_k}=\left(\tilde{\mathbf{A}}_m^T\mathbf{Q}^{-1}\tilde{\mathbf{A}}_m\right)^{-1}\left(\tilde{\mathbf{A}}_m^T\mathbf{Q}^{-1}\tilde{\mathbf{A}}_m+\mathbf{C}\mathbf{Q}_{\hat{\mathbf{N}}}\mathbf{C}^T\right)\left(\tilde{\mathbf{A}}_m^T\mathbf{Q}^{-1}\tilde{\mathbf{A}}_m\right)^{-1} \tag{11b}$$

where the medium variable

$$\mathbf{C}=\tilde{\mathbf{A}}_m^T\mathbf{Q}^{-1}\tilde{\mathbf{B}}\left(\mathbf{I}_n-\mathbf{Q}_{\hat{\mathbf{N}}}\mathbf{D}^T\mathbf{Q}_{\Delta\hat{\mathbf{N}}}^{-1}\mathbf{D}\right)\mathbf{Q}_{\hat{\mathbf{N}}} \tag{11c}$$

The second approach is to estimate 3D position states with the fixed DD ambiguities, then to determine the clock parameters with the known position states. It can be proved that the 4D solutions computed by equation (11a) are equivalent to those computed in the traditional 3D RTK model using DD measurements with fixed DD ambiguities. This equivalence allows simplification of the algorithms. We can alternatively realize the 4D RTK procedure based on the existing functions of 3D RTK.

The DD linear model is

$$\mathbf{H}\delta X_m=\mathbf{U},\ \ \mathbf{Q}_{DD}=\mathbf{D}\mathbf{Q}\mathbf{D}^T \tag{12}$$

where

$$\mathbf{H}=\begin{bmatrix}\mathbf{D}\mathbf{A}_m\\ \mathbf{D}\mathbf{A}_m\end{bmatrix},\ \ \mathbf{U}=\begin{bmatrix}\mathbf{D}\mathbf{L}_m+\lambda\Delta\breve{\mathbf{N}}\\ \mathbf{D}\mathbf{P}_m\end{bmatrix}.$$

After DD ambiguities are fixed by Eq.(8) in above procedure, we solve the coordinates based on the normal equations of DD model (12) are

$$\delta X_m=\left(\mathbf{H}^T\mathbf{Q}_{DD}^{-1}\mathbf{H}\right)^{-1}\mathbf{H}^T\mathbf{Q}_{DD}^{-1}\mathbf{U} \tag{13}$$

Substituting δX_m into equation (3) yields

$$\tilde{\mathbf{y}}_k=\begin{bmatrix}\tilde{\mathbf{A}}_k & \tilde{\mathbf{B}}\end{bmatrix}\begin{bmatrix}\delta T_k\\ \mathbf{N}_C\end{bmatrix}+\boldsymbol{\varepsilon}_{\mathbf{y}_k} \tag{14}$$

where

$$\tilde{\mathbf{y}}_k=\mathbf{y}_k-\begin{bmatrix}\mathbf{A}_k\\ \mathbf{A}_k\end{bmatrix}\delta X_m \text{ and } \tilde{\mathbf{A}}_k=\begin{bmatrix}1\\ 1\end{bmatrix}\otimes\mathbf{e}.$$

It is noticed that the SD ambiguities in Eq.(12) have constrained by integer DD ambiguities because the coordinates with DD integer ambiguities have been applied. The normal equations for the *k*th epoch are obtained

$$\begin{bmatrix}\tilde{\mathbf{A}}_k^T\mathbf{Q}^{-1}\tilde{\mathbf{A}}_k & \tilde{\mathbf{A}}_k^T\mathbf{Q}^{-1}\tilde{\mathbf{B}}\\ \tilde{\mathbf{B}}^T\mathbf{Q}^{-1}\tilde{\mathbf{A}}_k & \tilde{\mathbf{B}}^T\mathbf{Q}^{-1}\tilde{\mathbf{B}}\end{bmatrix}\begin{bmatrix}\delta T_k\\ \mathbf{N}_C\end{bmatrix}=\begin{bmatrix}\tilde{\mathbf{A}}_k^T\mathbf{Q}^{-1}\tilde{\mathbf{y}}_k\\ \tilde{\mathbf{B}}^T\mathbf{Q}^{-1}\tilde{\mathbf{y}}_k\end{bmatrix} \tag{15}$$

The equivalent normal equations for SD ambiguities N is derived

$$\tilde{\mathbf{B}}^T\mathbf{Q}^{-1}\mathbf{R}_k\tilde{\mathbf{B}}\hat{\mathbf{N}}_C=\tilde{\mathbf{B}}^T\mathbf{Q}^{-1}\mathbf{R}_k\tilde{\mathbf{y}}_k \tag{16})$$

Similarly, we solve the precise SD ambiguities using the most recent *m* epochs

$$\hat{\mathbf{N}}_C=\left(\tilde{\mathbf{B}}^T\mathbf{Q}^{-1}\sum_{k=1}^{m}\mathbf{R}_k\tilde{\mathbf{B}}\right)^{-1}\tilde{\mathbf{B}}^T\mathbf{Q}^{-1}\sum_{k=1}^{m}\mathbf{R}_k\tilde{\mathbf{y}}_k \tag{17}$$

Once the SD ambiguity $\hat{\mathbf{N}}_C$ is solved, we substitute it into equation (15) to compute the clock solution at the current epoch:

$$\delta\hat{T}_m=(\tilde{\boldsymbol{A}}_m^T\boldsymbol{Q}^{-1}\tilde{\boldsymbol{A}}_m)^{-1}\tilde{\boldsymbol{A}}_m^T\boldsymbol{Q}^{-1}(\tilde{\boldsymbol{y}}_m-\tilde{\boldsymbol{B}}\hat{\boldsymbol{N}}_c) \tag{18}$$

Referring to the discussions followed from (6b) and (6c), computations (16) to (18) can consider also adding and removing satellites.

Considering $\tilde{\mathbf{A}}_k=\begin{bmatrix}\mathbf{e}\\ \mathbf{e}\end{bmatrix}$ and simply assuming $\boldsymbol{Q}_L=\boldsymbol{I}_n$ and $\mathbf{Q}_P=\sigma_P^2/\sigma_0^2\times\mathbf{Q}_L=\beta\mathbf{I}_n$, where $\beta=\sigma_P^2/\sigma_0^2$, we can derive the simple formulae for this case

$$\delta\hat{T}_m=\frac{1}{n}\frac{\beta}{\beta+1}\sum_{i=1}^{n}(L_{m,i}+\frac{1}{\beta}P_{m,i}-\lambda\hat{N}_C) \tag{19}$$

In the case when the user 3D position states are known, i.e., the solutions with and without the constraints of DD integers are consistent. For simplicity purpose, the constraints of DD integers are not considered, then the cofactor matrix (6b) and constant term (6c) of SD ambiguities become

$$\mathrm{Q}_{\hat{\mathrm{N}}}=\frac{1}{\lambda^2\mathrm{m}}\left(\mathrm{I}_\mathrm{n}+\frac{\beta}{\mathrm{n}}\mathbf{e}\mathbf{e}^\mathrm{T}\right) \tag{20a}$$

$$\mathrm{w}=\lambda\sum_{\mathrm{k}=1}^{\mathrm{m}}[\mathrm{L}_\mathrm{k}-\mathbf{e}\mathbf{e}^\mathrm{T}(\frac{\mathrm{L}_\mathrm{k}}{\mathrm{n}}+\frac{\mathrm{P}_\mathrm{k}}{\mathrm{n}\beta})/(1+\frac{1}{\beta})] \tag{20b}$$

The LS estimate of the SD ambiguity parameters is given as

$$\hat{\mathrm{N}}=\mathrm{Q}_{\hat{\mathrm{N}}}\mathrm{w} \tag{20c}$$

Of course, we can fix the DD ambiguities by Eq.(8) and compute the SD ambiguities with DD integer ambiguity constraints by Eq.(10a) and (10b).
In general β is significantly larger than n, thus the variance for each element of N in Eq(20a) can be approximated as

$$\sigma_0^2\lambda^2 Q_{\hat{N}(i)} \approx \frac{\sigma_P^2}{m \cdot n} \quad (21b)$$

It is noted that in the formation of the LS equations (6a)-(6d) and (17)-(21b), the possible temporal correlation of SD code and phase measurement errors has not been taken into consideration. We also observe from (19) that although theoretically all SD ambiguities N_C may be estimated from time to time, larger uncertainties in the new rising satellites may affect the accuracy of the clock solutions. This suggests that the estimation of the clock biases may use phase and code measurements from selected satellites instead of all.

From the above derivations one can easily conclude that with known baselines or user stations, the RTK clock solutions can be determined directly from the SD phase and code measurements. The DD phase integer ambiguity resolution is not required unless very high accuracy is expectable. This simplifies the 4D RTK to RTK timing. Precise time synchronization over large distance is made easy as a long as the ionospheric and tropospheric biases in SD phase measurements are adequately corrected.

3. Corrections for inter-frequency biases in relative clock solutions

The hardware and signal processing architecture of a GNSS receiver will introduce frequency-dependent biases in the pseudorange and carrier phase measurements. These variations in the measurements, which may be different for code and phase, are commonly known as inter-frequency biases (Petovello et al., 2010). These biases are classified into two types: satellite-specific and receiver specific biases. A one-way pseudo-range or phase GPS measurement is defined as the pseudo-range or phase measurement for one receiver-to-satellite pair, which may also be called a "line-of-sight (LOS)" measurement or "zero difference" measurement. In the dual-frequency GPS case, four measurement equations are written as follows

$$p_{1,i}^j = \tilde{\rho} + I_1 + T_g^j + \varepsilon_{p1} \quad (22a)$$

$$p_{2,i}^j = \tilde{\rho} + \alpha I_1 + \alpha T_g^j + R_i + \varepsilon_{p2} \quad (22b)$$

$$\phi_{1,i}^j = \tilde{\rho} - I_i + T_g^j + \lambda_1 b_1 + \varepsilon_{\phi 1} \quad (22c)$$

$$\phi_{2,i}^j = \tilde{\rho} - \alpha I_i + \alpha T_g^j + \lambda_2 b_2 + R_i + \varepsilon_{\phi 2} \quad (22d)$$

where $p_{1,i}^j$, $p_{2,i}^j$ $\phi_{1,i}^j$ $\phi_{2,i}^j$ are the pseudoranges and phase measurements on L1 and L2 carriers respectively. The superscript j and subscript i, represent the jth satellite and the ith receiver; $\tilde{\rho}$ is the pseudorange, consisting of the geometric distance between the receiver and satellite, and receiver and satellite clock biases; $\lambda_1 b_1$ and $\lambda_2 b_2$ are the phase ambiguities in the carrier phase observables on L1 and L2 respectively, which are non-integers in the one-way phase, where λ_1 and λ_2 are the respective wavelengths for L1 and L2 carriers; T^j_g is the transmitter specific inter-frequency bias in the code measurements on L1 for the jth satellite; αT^j_g is the transmitter specific inter-frequency bias in the code measurements on L2 for the jth satellite, where $\alpha = (f_1/f_2)^2 = (77/60)^{2;}$ R_i is the receiver differential inter-frequency bias on L2 for the ith receiver. Because the timing of the GPS receives depends on the L1 C/A code, the inter-frequency bias on L1 is by definition zero; ε_{p1}, ε_{p2} are the pseudo-range noises for p1 and p2 respectively. The noise terms in this context include effects of multipath and receiver noise; $\varepsilon_{\phi 1}$, $\varepsilon_{\phi 2}$ are the carrier phase noises on L1 and L2 respectively. The noise terms in this context include effects of multipath and receiver noises.
The effects of the inter-frequency biases in the SD pseudorange and phase equations (1) and (2) are not explicitly shown up, but they indeed affect the relative clock results of interest, depending the measurements used. Table 1 summarizes the bias terms in different phase and code combinations in ZD and SD measurements. In DD measurements, all the receiver-specific and satellite-specific biases are cancelled. It is observed that in the ionosphere-free code and phase measurements, the satellite-specific bias T_g will be completely deleted, but the receiver-specific bias exists in both ionosphere-free SD code and phase measurements. Because the receiver-specific biases are generally stable over time, the biases in SD code and phase measurements can be pre-calibrated for a particular receiver-pair using zero or very short-baselines on regular basis.

4 Experiments and Analysis

We use one GPS data set to demonstrate the performance of the relative clock solutions with the proposed 4D RTK method. Table 2 summarizes the information about the data and settings in the 4D RTK data processing. Figure 1 (a) plots the 8 L1 SD phase ambiguity solutions (fractional) obtained using L1 and P1 code measurements and following the equations (17) and (18). It is clearly seen that within the few minutes of observations, the SD phase biases fall within 0.3 cycles; beyond 150th epoch (about 38 min for 15s simple intervals), each SD solution is stabilized within 0.1 cycle. Figure 1(b) plots the same SD

phase biases solutions obtained using L1 phase and the combined P12 code measurements. The section (b) shows the convergence of the solutions similar to (a), but there are a difference between the P1 and P12-based solutions in both integer and fractional components, presumably due to the receiver inter-frequency biases (IFB), which remains constant over hours to days, can possibly be corrected beforehand according to the Table 1.

Table 1: Influence of inter-frequency biases on the ZD, SD and DD

Combination	Bias term in ZD	Bias in SD
ϕ_1	T_g	0
$\phi_{12} = \frac{f_1\phi_2 - f_2\phi_2}{f_1 - f_2}$	$-\frac{f_1}{f_2}T_g - \frac{f_2 R}{f_1 - f_2}$	$-\frac{f_2 \Delta R}{f_1 - f_2}$
$\phi_c = \frac{f_1^2\phi_1 - f_2^2\phi_2}{f_1^2 - f_2^2}$	$\frac{f_2^2 R}{f_1^2 - f_2^2}$	$\frac{f_2^2 \Delta R}{f_1^2 - f_2^2}$
p1	Tg	0
$p_{12} = \frac{f_1 p_2 + f_2 p_2}{f_1 + f_2}$	$\frac{f_1}{f_2}T_g + \frac{f_2 R}{f_1 + f_2}$	$\frac{f_2 \Delta R}{f_1 + f_2}$
$p_c = \frac{f_1^2 p_1 - f_2^2 p_2}{f_1^2 - f_2^2}$	$\frac{f_2^2 R}{f_1^2 - f_2^2}$	$\frac{f_2^2 \Delta R}{f_1^2 - f_2^2}$
Note: ΔR is the receiver-specific bias with respect to the base receiver.		

Table 2. Experimental data and setting in the 4D RTK data processing

	Data Set and setting
Source of data	http://www.ngs.noaa.gov/CORS/cors-data.html, RINEX data: Sites: P474-P478 on 1/1/2007
Observation types	L1, L2, P1,P2
Distance	21km
Cutoff elevation	15 degrees
Number of SVs	8
Data period	00:09:30~01:36:00
Sample rate	15 seconds
Total of epochs	347
Code noise P1,P2 (SD)	0.363m (estimated)
Phase noise L1,L2 (SD)	0.010cm (estimated)

Figure 2 (a) plots the RTK clock solutions against the DGPS clock solutions using the P12 code measurements, with the differences as shown in Figure 2 (b). The effects of the receiver dependent inter-frequency biases on the relative clock solutions depend on the combination of the code measurements. Figure 3 (a) plots the RTK clocks derived from P1 and P12 code measurements respectively, and the difference between two RTK clocks are shown in Figure 3 (b), which tends to converge when the data is cumulating.

.

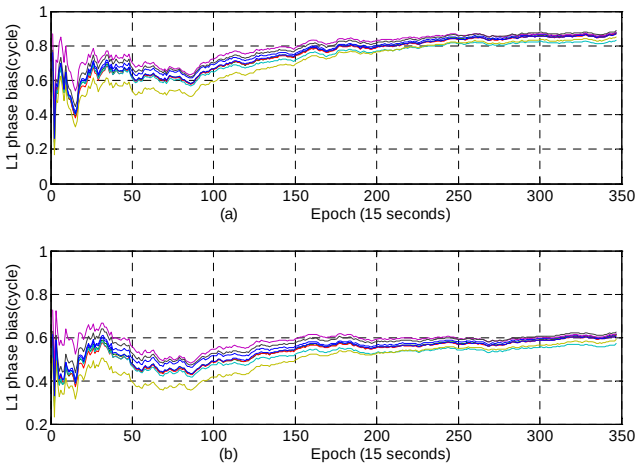

Figure 1. Illustration of the L1 SD phase bias solutions (fractional) obtained using L1 and P1 code measurements in section (a) and using L1 and P12 codes in section (b) respectively. The results follow from the equations (20) and (21). It is clearly seen that within the first minutes, the variation of SD estimates are confined 0.3 cycles; beyond 150th epoch (about 38 min for 15 simple intervals), each SD solution is then stabilized within 0.1 cycle.

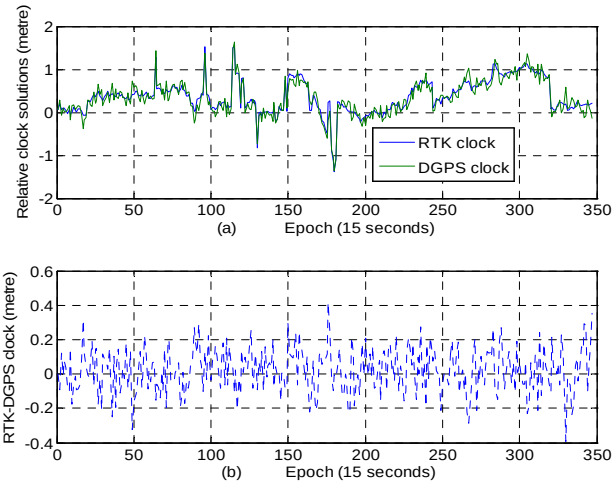

Figure 2. Comparison between RTK and DGPS clock solutions using P12 code measurements in section (a) and differences are shown in section (b).

As shown in the observation equation (1), the accuracy of the RTK clock solutions is dominated by two factors: (1) the overall SD phase noise level, which may include the effects of ionosphere, tropospheric and random noise and multipath and (2) the uncertainty of the SD phase bias solutions being improved from time to time. In Figure 4

(a), we show the code STD variations and the overall STD of code P1 and P12 are 0.363m and 0.263 m respectively. The overall noise of the L1 SD phase observations is estimated to about 1.0 cm considering both ionospheric and tropospheric effects. As a result, the accuracy of the RTK clock solutions are plotted in Figure 4 (b), showing the RTK clock accuracy convergence to the level of 1.5 cm beyond the 150th epochs

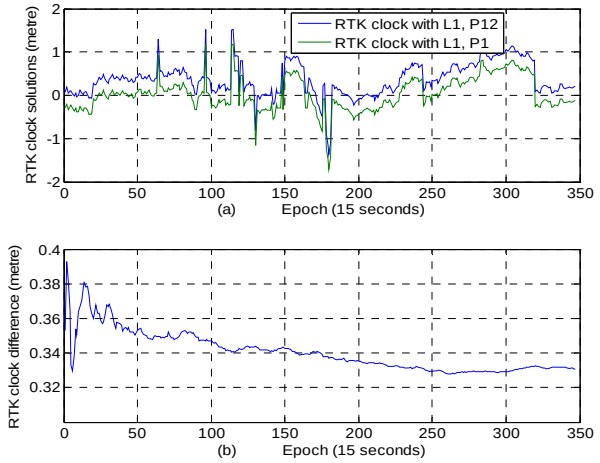

Figure 3. Comparison between two RTK clock solutions obtained with (L1,P1) and (L1,P12) respectively, showing the effects of the receiver-frequency related biases.

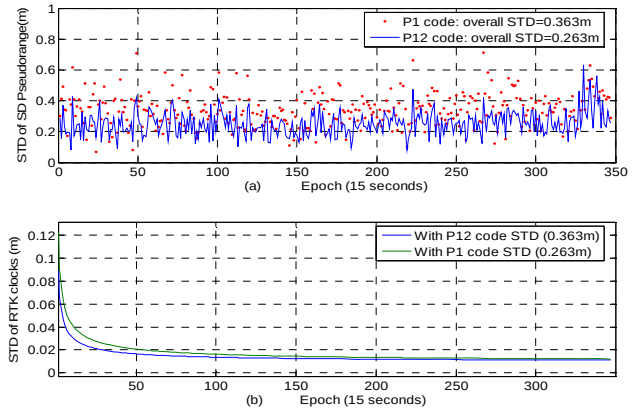

Figure 4 (a) Illustrations of the code STD variations and the overall STD of code P1 and P12 are 0.363m and 0.263 m respectively. The accuracy of the RTK clock solutions reaches the level of 3 cm within a few minutes, and converges to 1.5 cm beyond the 150th epoch.

5. CONCLUSIONS

This paper has developed the 4 D RTK positioning and timing models and algorithms that can generate the relative clock solutions along with 3D position states. The existing 3D RTK model use DD code and phase measurements is a equivalently reduced case of the 4D RTK problem, but eliminating the receiver clock errors. The proposed 4D RTK model has been based on SD measurements between receivers. While the user 3D position states are determined as usual with the DD phase measurements whose integer ambiguities are searched and fixed using the existing ILS procedure, the relative clock bias and the SD phase ambiguities are estimated simultaneously epoch by epoch with the SD code and phase observations. The constant nature of the SD phase ambiguity parameters allows their estimations to be improved accumulatively; in turn the relative clock solutions are improved from time to time without clock modeling. When the user baselines or user coordinates are accurately known, the RTK clock solutions can be determined directly from the SD phase and code measurements. As the DD phase integer ambiguity resolution is no longer required, 4D RTK is reduced to RTK timing. Precise time synchronization over large distance thus is thus made easy.

Experimental analysis performed with a GPS data set collected over a 21 km baseline at 15 seconds have shown that within the first minutes of observations, the SD phase biases fall within the range of 0.3 cycles, achieving a 0.2 ns clock uncertainty. Beyond 150 epochs, the SD phase biases are stabilized within the range of +/-1.5 cm, thus leading the clock biases estimation to the precision and accuracy of better than 0.1 ns, which have included the effect of the errors in the SD phase measurements.

ACKNOWLEDGEMENTS

This work was carried out under the partial financial support of the Australian Cooperative Research Centre for Spatial Information project. The contribution from the second author was made during his PhD candidature at Tongji University in China in early 2010.

REFERENCES

Allan, D W. and Weiss, M. A. (1980) Accurate Time and Frequency Transfer During the Common View of a GPS Satellite, Proceedings of 34th Annul Frequency Control Symposium, 1980,p334-346.

Bauch A., Achkar J., Bize S., Calonico D., Dach R., Hlavac R., Lorini L., Parker T., Petit G., Piester D., Szymaniec K., and Uhrich P. (2006) Comparison between frequency standards in Europe and USA at the 10–15 Uncertainty Level, Metrologia, 2006,43:109–120.

Orgiazzi, D, F. Lahaye, G. Cerretto and P. Tavella (2006) GPS time transfer: using precise point positioning for clock comparisons, GPS World, November 1, 2006.

Klepczyniski, W. J (1996) GPS for Precise Time and Time Interval Measurement, Global Positioning Systems: Theory and Applications: Volume II (eds by B Parkinson, J Spilker Jr), p483-500

Kouba J. and Héroux P. (2001) Precise point positioning using IGS orbit and clock products, GPS Solutions, 2001, 5(2):12–28.

JPL website (2010): http://www.gdgps.net/products/orbit-clock-states.html

Lewandowski, W. and Thomas, C (1991) GPS Time Transfer, Proceedings of the IEEE, VOL. 79, NO. 7, JULY 1991, p991-1000.

Miranian, G., and Klepczyniski, W. J. Time Transfer via GPS at USNO, Proceedings of ION GPS 91, Institute of Navigation,, Washington DC, Sept 1991.

Parker T. and Matsakis D. (2004) Time and frequency dissemination: advances in GPS transfer techniques, GPS World, 2004, 15(11):32–38.

Ray J. and Senior K. (2003) IGS/BIPM Pilot Project: GPS carrier phase for time/frequency transfer and timescale formation, Metrologia, 2003, 40:S270–S288.

Ray J. and Senior K. (2002) New IGS clock products: A global time transfer assessment, GPS World, 2002, 13(11): 45–51.

Schildknecht T. and Dudle D. (2000) Time and frequency transfer: high precision using GPS phase measurements, GPS World, 2000, 11(2):48–52.

Petovello, M, F Takac, GNSS solutions: Glonass inter-frequency biases and ambiguity resolution, Indside GNSS, March/April, 2009, p24-28